Supplement of The Cryosphere, 15, 4655–4673, 2021
https://doi.org/10.5194/tc-15-4655-2021-supplement

The Cryosphere Open Access

Supplement of

Did Holocene climate changes drive West Antarctic grounding line retreat and readvance?

Sarah U. Neuhaus et al.

Correspondence to: Sarah U. Neuhaus (suneuhau@ucsc.edu)

Supplement

1 Radiocarbon Model Methods

We develop a two-phase model of ^{14}C and ^{12}C to examine the timing of grounding line retreat and readvance for our field sites. We calculate the evolution of ^{14}C and ^{12}C separately. The first phase of the model represents the time after the grounding line retreated beyond our sites, and the second represents the time after the grounding line had readvanced. To model the concentration of ^{14}C, n, in the first phase of our model (exposure to seawater), we assume that radiocarbon is being added to the sediments at a constant rate, a, while a fraction of this unstable radioisotope decays:

$$\frac{\partial n}{\partial t} = a - \lambda n \tag{S1}$$

Where λ is the decay constant and t is time. To simplify our calculations, we substitute:

$$k = -\lambda = -\frac{1}{\tau} \tag{S2}$$

Where τ is the mean lifetime of ^{14}C (8033 years). Eq. (S2) thus simplifies to:

$$\frac{\partial n}{\partial t} = a + kn \tag{S3}$$

We integrate Eq. S3 using the integrating factor method and multiply both sides of the equation by the factor e^{-kt}:

$$e^{-kt}\frac{\partial n}{\partial t} - e^{-kt}kn = ae^{-kt} \quad \text{(S4)}$$

Remembering the product rule, we observe that this operation transforms the left-hand side of Eq. (S4) into a derivative of the product of n and the integrating factor, such that:

$$\left(e^{-kt}n(t)\right)' = ae^{-kt} \quad \text{(S5)}$$

We obtain a definite integral of both sides of Eq. (S5) using a dummy variable of integration, ξ.

$$\int_{\xi=0}^{\xi=t} \left(e^{-k\xi}n(\xi)\right)' d\xi = \int_{\xi=0}^{\xi=t} ae^{-k\xi} d\xi \quad \text{(S6)}$$

Which results in:

$$n(t)e^{-kt} + n_o = a\left(\frac{1-e^{-kt}}{k}\right) \quad \text{(S7)}$$

We assume that $n_o = 0$ because the sediments have been isolated for long enough that there should be no significant radiocarbon present at the moment the grounding line retreated past our sediment sampling sites, exposing them to accumulation of radiocarbon at rate a. Recognizing this, solving for $n(t)$, and substituting for k using Eq. (S2) we obtain the final equation for changes in ^{14}C concentration in phase 1 of the model:

$$n(t) = a\tau\left(e^{\frac{t}{\tau}} - 1\right)e^{\frac{-t}{\tau}} = a\tau\left(1 - e^{\frac{-t}{\tau}}\right) \quad \text{(S8)}$$

To model the evolution of the most abundant and stable isotope of carbon, ^{12}C, we assume that it was also being added at a constant rate, A, during phase one when the sediments at the sampling sites were exposed to seawater after grounding line retreat. This time, the initial amount of ^{12}C (N_o) is not assumed to be negligible, due to inheritance of radiocarbon dead organic matter in subglacial sediments from the region, including any ^{12}C that may have been incorporated during subglacial erosion (Tulaczyk et al., 1998):

$$N(t) = N_o + At \quad \text{(S9)}$$

In the second phase of the model, when the ice sheet has readvanced over our sediment sampling sites, we assume that the addition of carbon ceases. Hence, the amount of ^{12}C is no longer changing but ^{14}C is experiencing decay, following the standard equation:

$$n(t) = n^{*} e^{\frac{-t}{\tau}} \tag{S10}$$

Where n^* is the value of n at the time of ice sheet re-grounding over a field site (when the model switches from phase one to phase two). The results for all cores are shown in Fig. S1.

We performed sensitivity tests to examine how changing the rate of ^{12}C addition would affect the timing of grounding line retreat over our field sites. In our radiocarbon model, we assume that ^{12}C is deposited at a constant rate during phase 1, and that there is no additional carbon input in phase 2. To test how varying the rate of ^{12}C input (A) during phase 1 would affect the timing of grounding line retreat we increased A by 1% every time step (100 years). The differences in the number of model matches from the runs where A was kept constant and the runs when A increased every 100 years are shown in Fig. S2. Increasing the rate of ^{12}C addition did not alter the timing of grounding line retreat noticeably. The timing of grounding line retreat over SLW, WIS, KIS, and BIS was 4300^{+1500}_{-2500} years ago, 4600^{+1600}_{-2200} years ago, 1800^{+2700}_{-700} years ago, and 1700^{+2900}_{-600}years ago, respectively. To test how adding ^{12}C during phase 2 would affect the timing of grounding line retreat, we added 10^{-7} g of ^{12}C every timestep (100 years). The differences in model runs where ^{12}C was not added and runs where it was are shown in Fig. S3. This also did not alter the timing of grounding line retreat noticeably. The timing of grounding line retreat over SLW, WIS, KIS, and BIS was 4300^{+1500}_{-2500} years ago, 4700^{+1500}_{-2300} years ago, 1800^{+2700}_{-700} years ago, and 1700^{+2800}_{-600} years ago, respectively.

2 Temperature Model Methods

We also develop a two-phase model of temperature evolution through ice to compare to observed basal temperature gradients. Phase 1 of the model represents the time when the ice is assumed to have been part of a floating ice shelf, and phase 2 represents the time after the ice shelf has grounded. For both phases we model the temperature profile through the ice using the vertical diffusion-advection equation:

$$\frac{\partial T}{\partial t} = \alpha^{*} \frac{\partial^2 T}{\partial t^2} - w \frac{\partial T}{\partial z} \tag{S11}$$

Where T is temperature in degrees Celsius, t is time, α^* is the diffusion coefficient, w is the vertical velocity, and z is depth from the ice surface. We calculate α^* for both phases using the equation:

$$\alpha^* = 33.8 - 0.3514T \tag{S12}$$

During phase 1, we model the temperature profile of a floating ice shelf, assuming a range of constant ice thicknesses between 500m and 1000m. We initialize the models with a linear temperature distribution through the ice, assuming the temperature at the ice surface to be -25 ºC (Engelhardt, 2004) and calculating the temperature of the ice at the base using the equation (modified from Begeman et al. [2018]):

$$T = 0.081 - 0.0568S - 6.858 \times 10^{-4}z \tag{S13}$$

Where S is the salinity, assumed to be 34 PSU from CTD profiles taken at WGZ (Begeman et al., 2018). We use an accumulation rate of 0.15 m/yr (Waddington et al., 2005), and assume a matching basal melt rate (m_b) to allow ice shelf thickness to remain constant throughout phase 1. Prior to selecting this basal melt rate we tested multiple values of basal melt rate, which we will discuss further below. Accumulation is equal to the sum of w and change in ice thickness (h). We allow the simulated ice shelf temperature profile to reach steady state, and then begin phase 2 of the model.

Using the resulting profile from phase 1 as the initial condition for phase 2 runs, we model the temperature profile through grounded ice using Eq. (S11) (phase 2). We assume accumulation to be the same (0.15 m/yr [Waddington et al., 2005]), but change the basal boundary condition to reflect the freezing temperature of freshwater ice in contact with fresh meltwater:

$$T = 0°\mathrm{C} - \left(6.858 \times 10^{-4}\,\frac{°\mathrm{C}}{m}\right)z. \tag{S14}$$

We allow the ice to thicken at the rate of 0.05 m/yr based on estimates from Joughin and Tulaczyk (2002), thus reducing the vertical velocity. In addition, we examined multiple combinations of h and w (Fig. S6), discussed below. We allow the model to run for 8,000 years, keeping track of the temperature gradient of the bottom 100 m for each year. We also measure basal accretion using the equation:

$$H_B = (k_T T_B - G)\left(\frac{1}{\rho_i L}\right) \tag{S15}$$

Where H_B is the annual change in basal ice thickness, k_T is the thermal conductivity of ice (assumed to be 2 W/m K here), T_B is the temperature gradient of the bottom 100 m of ice, G is the geothermal flux (assumed to be 0.07 W/m^2) here, ρ_i is the density of ice (assumed to be 895 kg/m^3 here), and L is the latent heat of fusion of water (3.34x10^5 J/kg). It should be noted that Eq. (S15) assumes negligible contribution of heat from basal shear heating.

We performed sensitivity tests to examine how altering our assumptions for w, h, and m_b affected the final basal temperature gradient. For phase 1, we first examined the scenario in which the ice shelf thickness remains unchanged. Thus, in this scenario accumulation equals both m_b and w (Fig. S4). For the four values of w (m_b) we examined (0 m/yr, 0.05 m/yr, 0.1 m/yr, and 0.15 m/yr), the model was able to reproduce all of the measured basal temperature gradients for all ice thicknesses only when w (m_b) = 0.15 m/yr (Fig. S4). Further analysis revealed that the m_b had to be a least 0.13 m/yr to reproduce the steep basal temperature gradients. When w = 0 m/yr, the total range for possible *Ti* for BIS, KIS, and UC was 200-100 years ago, 2400-100 years ago, and 3500-100 years ago, respectively. When w = 0.1 m/yr, the total range for possible *Ti* for BIS, KIS, and UC was 900-100 years ago, 2500-100 years ago, and 3500-100 years ago, respectively. When w = 0.05 m/yr, the total range for possible *Ti* for BIS, KIS, and UC was 1200-200 years ago, 2600-100 years ago, and 3500-100 years ago, respectively. When w = 0.15 m/yr, the total range for possible *Ti* for BIS, KIS, and UC was 1400-600 years ago, 2700-300 years ago, and 3600-100 years ago, respectively. Additionally, we examined multiple values of m_b (0 m/yr, 0.05 m/yr, 0.1 m/yr, and 0.15 m/yr), but kept surface accumulation equal to 0.15 m/yr and allowed the ice shelf to thicken in response to lower m_b (Fig. S5). Of the four values of m_b that we examined (0 m/yr, 0.05 m/yr, 0.1 m/yr, and 0.15 m/yr), the model only reproduced all measured basal temperature gradients when m_b = 0.15 m/yr. For m_b = 0 m/yr and m_b = 0.05 m/yr we were unable to reproduce any of the observed basal temperature gradients. Thus, we conclude that we are only able to reproduce the steep basal temperature gradients when basal melt rate of the ice shelf is high, i.e., at least comparable to the surface accumulation rate. When m_b = 0.1 m/yr, the total range of possible T_i for BIS, KIS, and UC was 200-100 years ago, 400-100 years ago, and 600-400 years ago, respectively. When m_b = 0.15 m/yr, the total range of possible T_i for BIS, KIS, and UC was 1400-600 years ago, 2700-300 years ago, and 3600-100 years ago, respectively.

We also performed sensitivity tests for w and h for the second phase of the model (Fig. S6). We tested multiple combinations of w and h: w = 0 m/yr, h=0.15 m/yr; w = 0.05 m/yr, h=0.1 m/yr; w = 0.1 m/yr, h=0.05 m/yr; w = 0.15 m/yr, h=0 m/yr. Because accumulation rate (which remained constant) is a sum of w and h, w and h are inversely related to each other. In each scenario we were able to reproduce all measured basal temperature gradients. The timing of T_i for the steepest basal temperature gradients remained largely unchanged by the changes in w and h. However, for the less steep basal temperature gradients, reducing the amount of ice thickening (h) increases the amount of time the ice has been grounded. Because ice thickening has been observed in this area (Joughin and Tulaczyk, 2002), we discount the possibility of a scenario in which no thickening is happening (h=0 m/yr). For the scenario in which w = 0 m/yr and h = 0.15 m/yr, the total range of possible T_i for BIS, KIS, and UC was 800-500 years ago, 1300-300 years ago, and 1600-100 years ago, respectively. For the scenario in which w = 0.05 m/yr and h = 0.1 m/yr, the total range of possible T_i for BIS, KIS, and UC was 1100-500 years ago, 1800-300 years ago, and 2300-100 years ago, respectively. For the scenario in which w = 0.1 m/yr and h = 0.05 m/yr, the total range of possible T_i for BIS, KIS, and UC was 1400-600 years ago, 2700-300 years ago, and 3600-100 years ago, respectively. For the scenario in which w = 0.15 m/yr and h = 0 m/yr, the total range of possible T_i for BIS, KIS, and UC was 2200-600 years ago, 4100-300 years ago, and 5400-100 years ago, respectively.

Finally, we examined how varying the geothermal flux would affect the thickness of basal ice in our calculations. In our temperature diffusion model, we assumed the geothermal flux to be a single value of 0.07 W/m^2, although measurements of geothermal flux in the Siple Coast and Ross Sea Embayment indicate that the geothermal flux can vary widely in this area: 285 ± 80 mW/m^2 at SLW (Fisher et al., 2015), 88 ± 7 mW/m^2 (Begeman et al., 2017), and 55 mW/m^2 at RISP (Foster, 1978). To test what effect varying the geothermal flux would have on basal ice thickness, we varied it by 10% (i.e. 0.07 ± 0.007 W/m^2). A geothermal flux of 0.077 W/m^2 produced basal ice thicknesses of 3.8 – 9.3 m, 2.2 – 14.0 m, and 0.9 – 16.7 m for BIS, KIS, and UC, respectively. A geothermal flux of 0.063 W/m^2 produced basal ice thicknesses of 4.6 – 11.2 m, 2.5 – 17.5 m, and 1.0 – 22.0 m for BIS, KIS, and UC, respectively. For comparison, the basal ice thicknesses produced for a geothermal flux of 0.07 W/m^2 were 4.2 – 10.2 m, 2.4 – 15.8 m, and 0.9 – 19.3 m for BIS, KIS, and UC, respectively. All these basal ice thicknesses are on par with observations of basal ice thickness in the Siple Coast region (Christoffersen et al., 2010; Vogel et al., 2005).

3 Ionic Diffusion Sensitivity Testing

In the ionic diffusion modelling of SLW, we assumed sediment porosity to be 40% based on observations of till from previous studies (Engelhardt et al., 1990; Tulaczyk et al., 2001). To test what effect this assumption had on our results, we ran the model with porosities of 30 % and 50%, and compared these results to our model results (Fig. S7). The total range for possible timing of grounding line readvance (T_i) over SLW was 2000 years ago to present assuming a porosity of 30%, and 1600 years ago to present assuming a porosity of 50%.

4 Carbon and Nitrogen Measurements

Total carbon (TC), total organic carbon (TOC), total inorganic carbon (TIC), carbon-to-nitrogen ratios, and $\delta^{13}C$ were measured at the University of California Santa Cruz Stable Isotope Laboratory. The results from those measurements are shown here (Table S1). In the two-phase model of radiocarbon we use measurements of total organic carbon (TOC) from sediment cores collected at our field sites to constrain our model results (see section 2.3). Carbon-to-nitrogen ratios and measurements of $\delta^{13}C$ were used to glean information about the sources of organic matter found in the sediments and about microbial communities living in the subglacial environments of our field sites.

References

Begeman, C. B., Tulaczyk, S. M. and Fisher, A. T.: Spatially Variable Geothermal Heat Flux in West Antarctica: Evidence and Implications, Geophys. Res. Lett., 44(19), 9823–9832, doi:10.1002/2017GL075579, 2017.

Begeman, C. B., Tulaczyk, S. M., Marsh, O. J., Mikucki, J. A., Stanton, T. P., Hodson, T. O., Siegfried, M. R., Powell, R.

D., Christianson, K. and King, M. A.: Ocean Stratification and Low Melt Rates at the Ross Ice Shelf Grounding Zone, J. Geophys. Res. Ocean., 123(10), 7438–7452, doi:10.1029/2018JC013987, 2018.

Christoffersen, P., Tulaczyk, S. and Behar, A.: Basal ice sequences in Antarctic ice stream: Exposure of past hydrologic conditions and a principal mode of sediment transfer, J. Geophys. Res. Earth Surf., 115(3), 1–12, doi:10.1029/2009JF001430, 2010.

Engelhardt, H.: Thermal regime and dynamics of the West Antarctic ice sheet, Ann. Glaciol., 39, 85–92, 2004.

Engelhardt, H., Humphrey, N., Kamb, B. and Fahnestock, M.: Physical conditions at the base of a fast moving Antarctic ice stream, Science (80-.)., 248(4951), 57–59, doi:10.1126/science.248.4951.57, 1990.

Fisher, A. T., Mankoff, K. D., Tulaczyk, S. M., Tyler, S. W. and Foley, N.: High geothermal heat flux measured below the West Antarctic Ice Sheet, Sci. Adv., 1(6), e1500093–e1500093, doi:10.1126/sciadv.1500093, 2015.

Foster, T. D.: Temperature and salinity fields under the Ross Ice Shelf International Weddell Sea Oceanographic Expedition , 1978, Antarct. J. [Of United States], (13), 81–82, 1978.

Joughin, I. and Tulaczyk, S.: Positive mass balance of the Ross Ice Streams, West Antarctica, Science (80-.)., 295(5554), 476–480, doi:10.1126/science.1066875, 2002.

Tulaczyk, S., Kamb, B., Scherer, R. P. and Engelhardt, H. F.: Sedimentary processes at the base of a West Antarctic ice stream; constraints from textural and compositional properties of subglacial debris, J. Sediment. Res., 68(3), 487–496, doi:10.2110/jsr.68.487, 1998.

Tulaczyk, S., Kamb, B. and Engelhardt, H. F.: Estimates of effective stress beneath a modern West Antarctic ice stream from till preconsolidation and void ratio, Boreas, 30(2), 101–114, doi:10.1111/j.1502-3885.2001.tb01216.x, 2001.

Vogel, S. W., Tulaczyk, S., Kamb, B., Engelhardt, H., Carsey, F. D., Behar, A. E., Lane, A. L. and Joughin, I.: Subglacial conditions during and after stoppage of an Antarctic Ice Stream: Is reactivation imminent?, Geophys. Res. Lett., 32(14), 1–4, doi:10.1029/2005GL022563, 2005.

Waddington, E. D., Conway, H., Steig, E. J., Alley, R. B., Brook, E. J., Taylor, K. C. and White, J. W. C.: Decoding the dipstick: Thickness of Siple Dome, West Antarctica, at the Last Glacial Maximum, Geology, 33(4), 281–284, doi:10.1130/G21165.1, 2005.

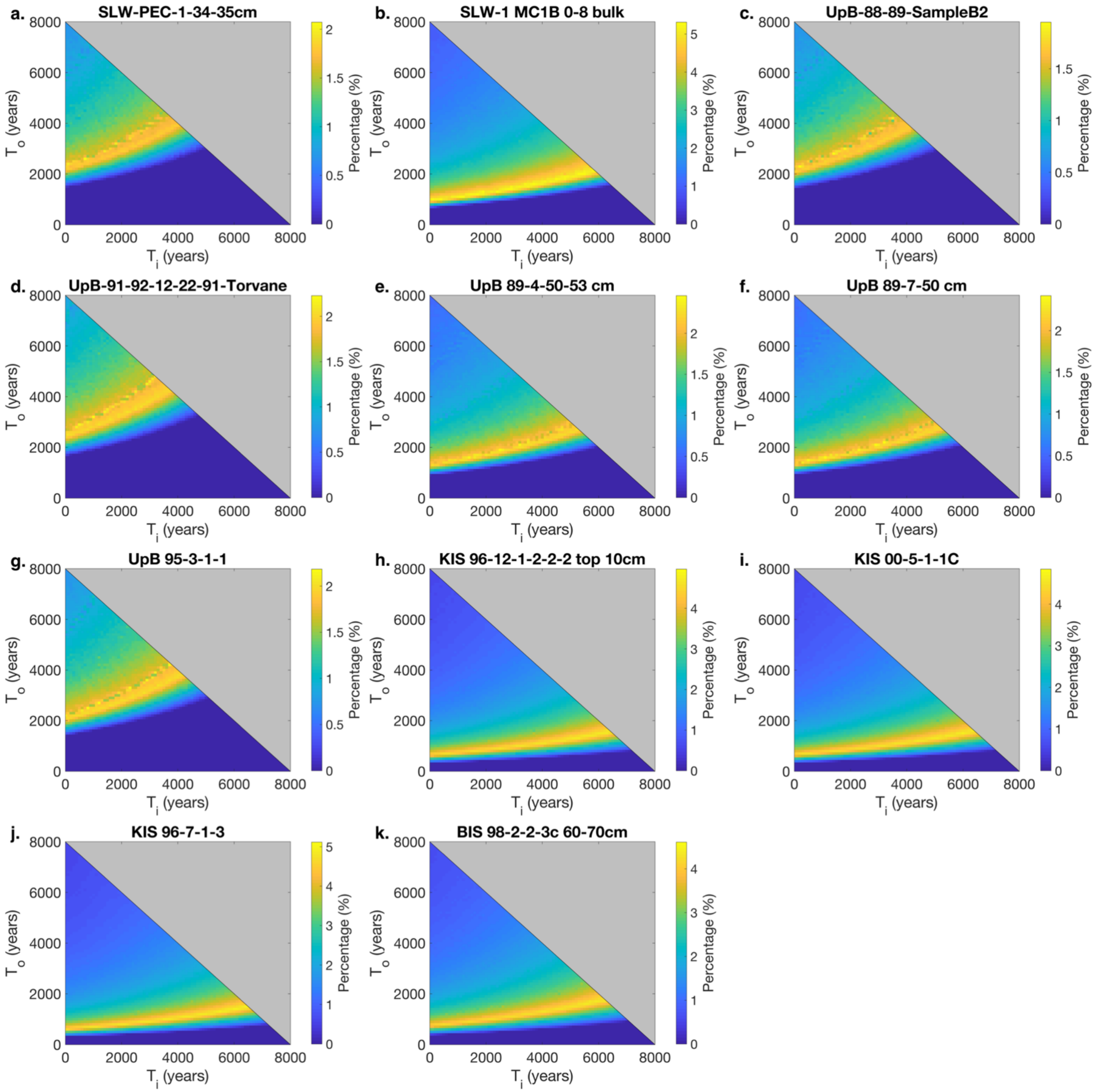

Figure S1: Results from radiocarbon modelling for each core individually. a) and b) are from SLW. c-g) WIS. h-j) KIS. k) BIS.

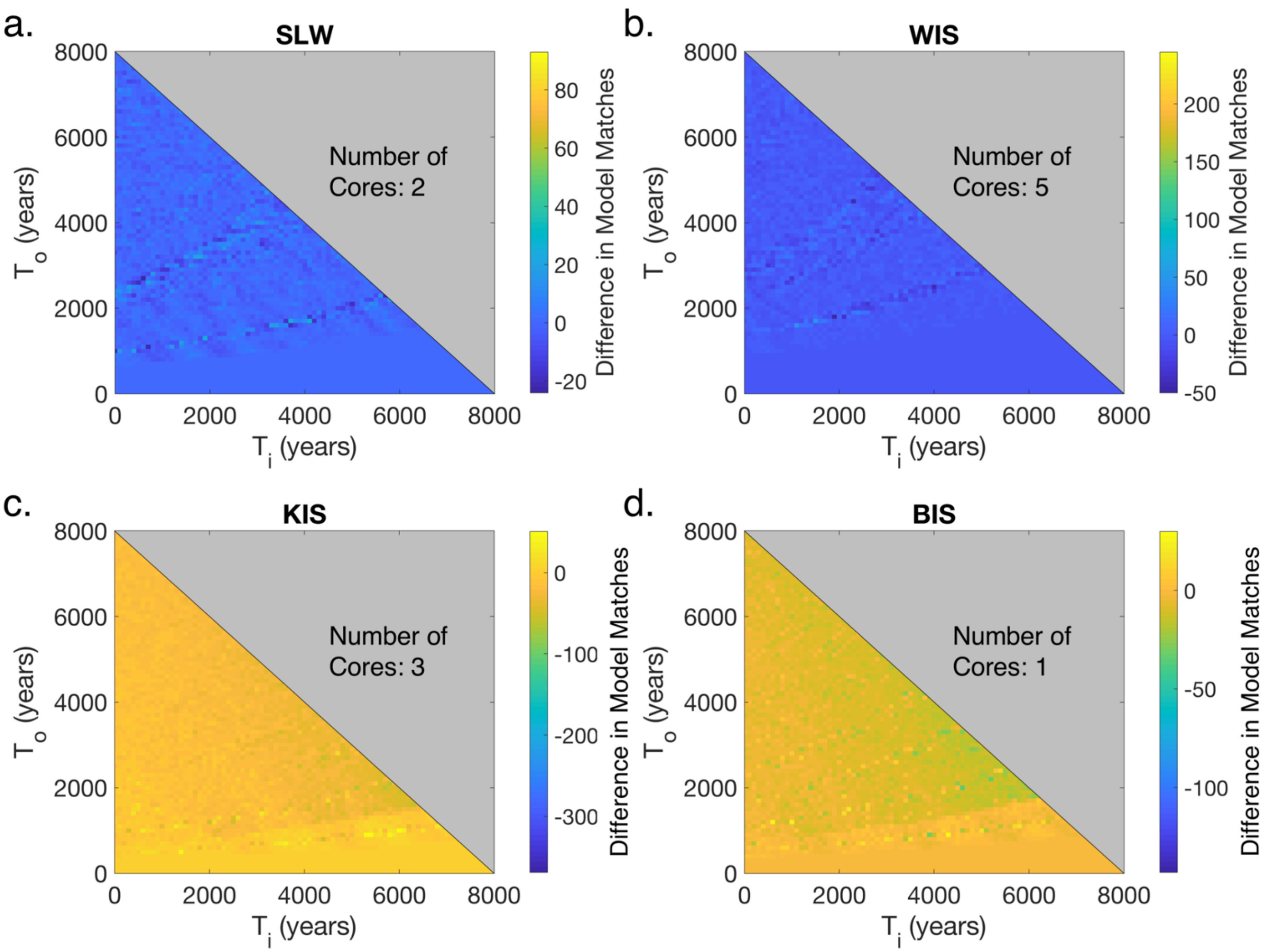

Figure S2: Sensitivity testing for phase 1 of the radiocarbon model. In this scenario, the rate of ^{12}C input (*A*) was increased by 1% every 100 years. a-d show the difference between the number model matches when *A* was kept constant and when *A* increased every 100 years.

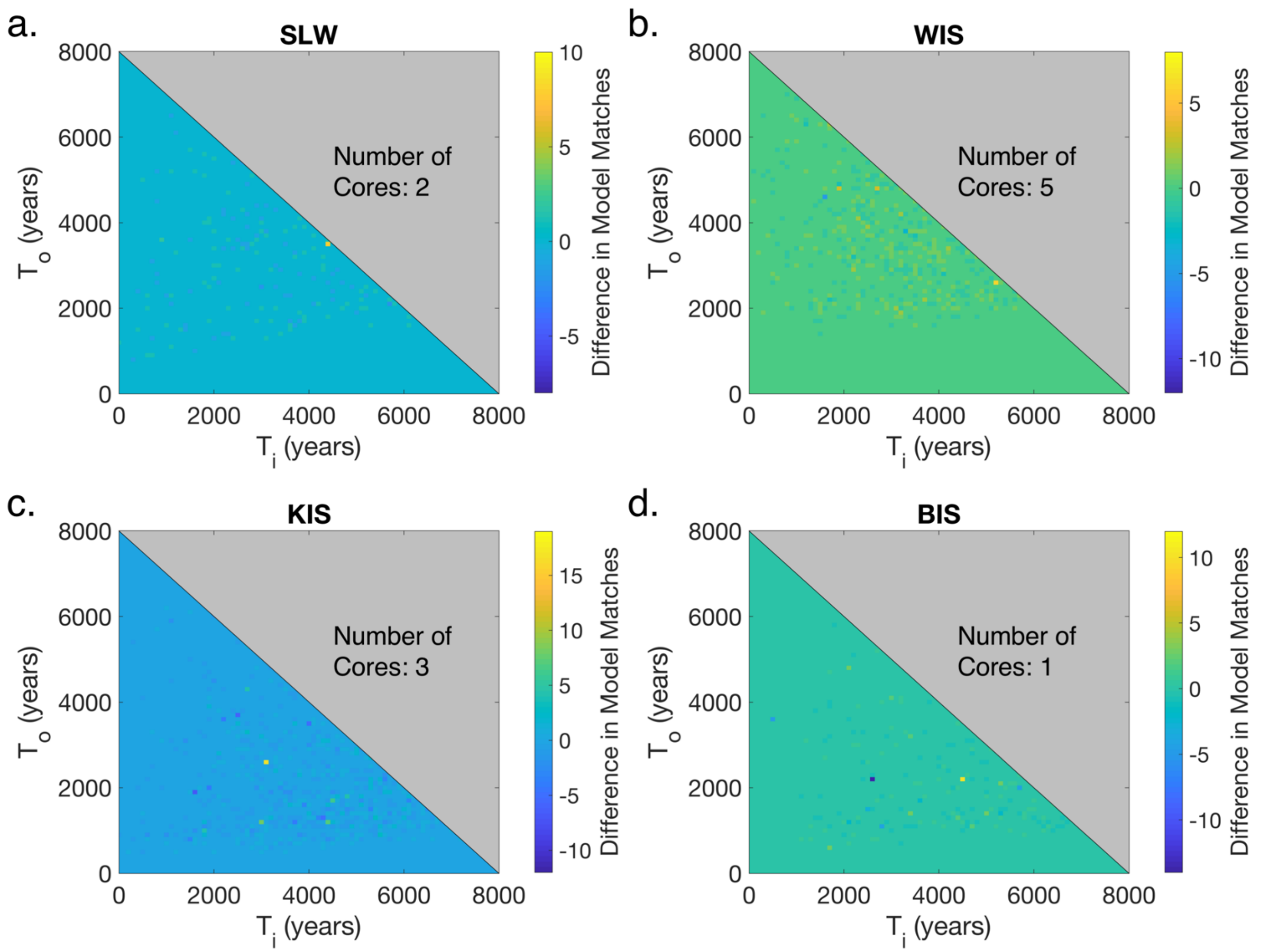

Figure S3: Sensitivity testing for phase 2 of the radiocarbon model. In this scenario, 10^{-7} g of ^{12}C was added to the sediments every 100 years. a-d show the difference between the number model matches when no ^{12}C was added, and when ^{12}C was added every 100 years.

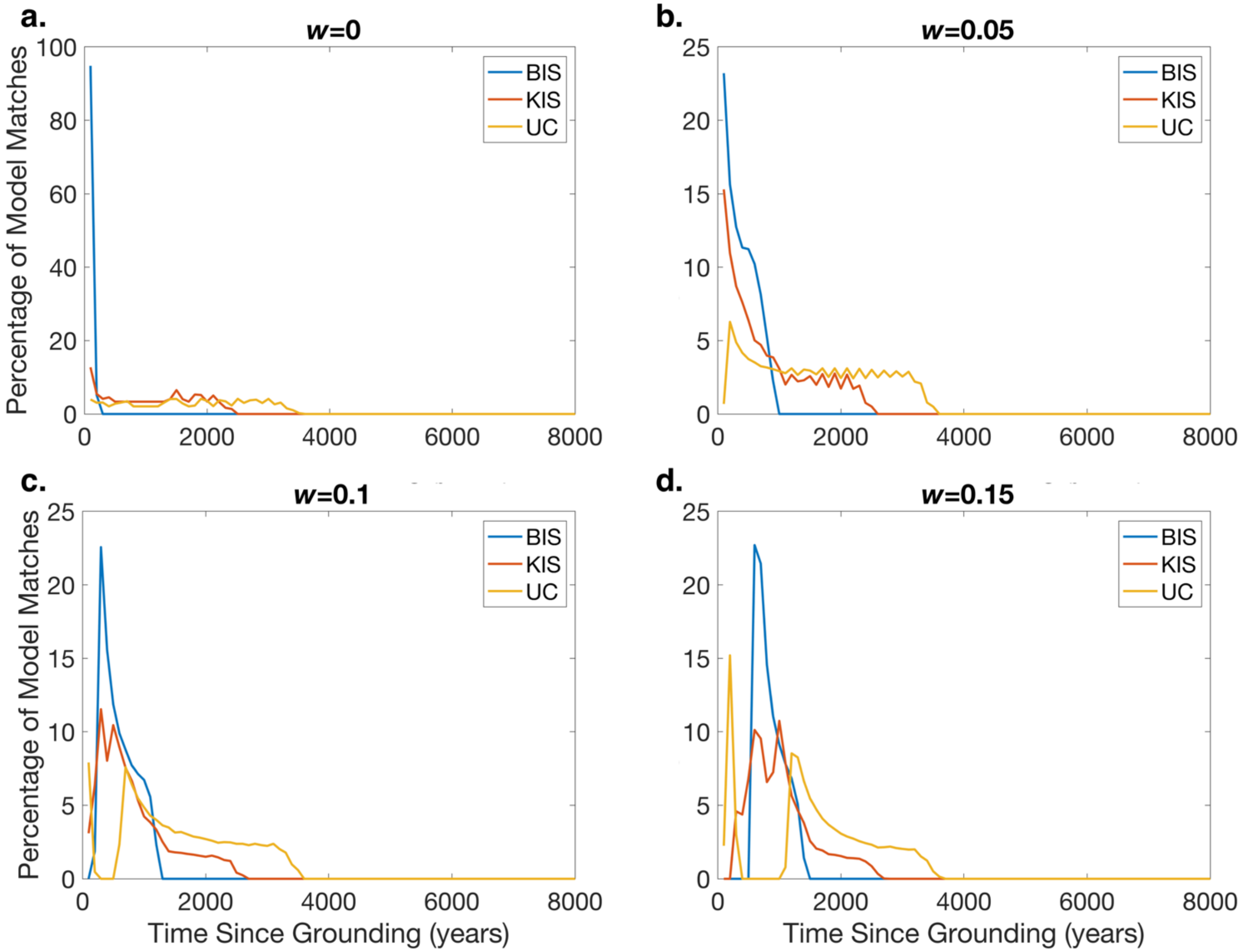

Figure S4: Sensitivity testing for phase 1 of ice temperature model. In this scenario, ice shelf thickness is kept constant. We examine multiple values of vertical velocity (*w*), and by extension multiple values of surface accumulation and basal melt.

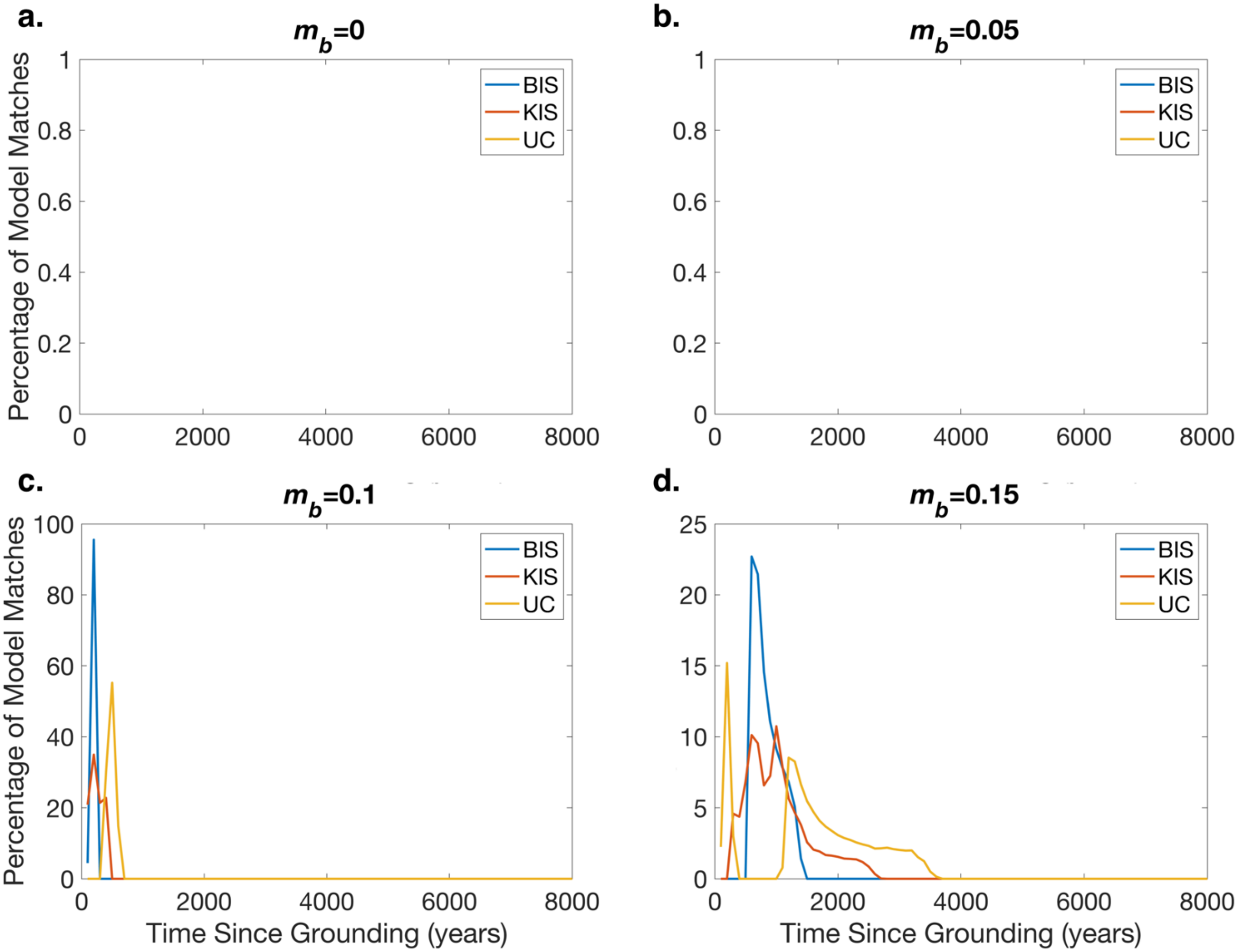

Figure S5: Sensitivity testing for phase 1 of the ice temperature model. In this scenario, we keep surface accumulation constant, but allow the ice shelf to thicken in response to lower rates of basal melt (m_b).

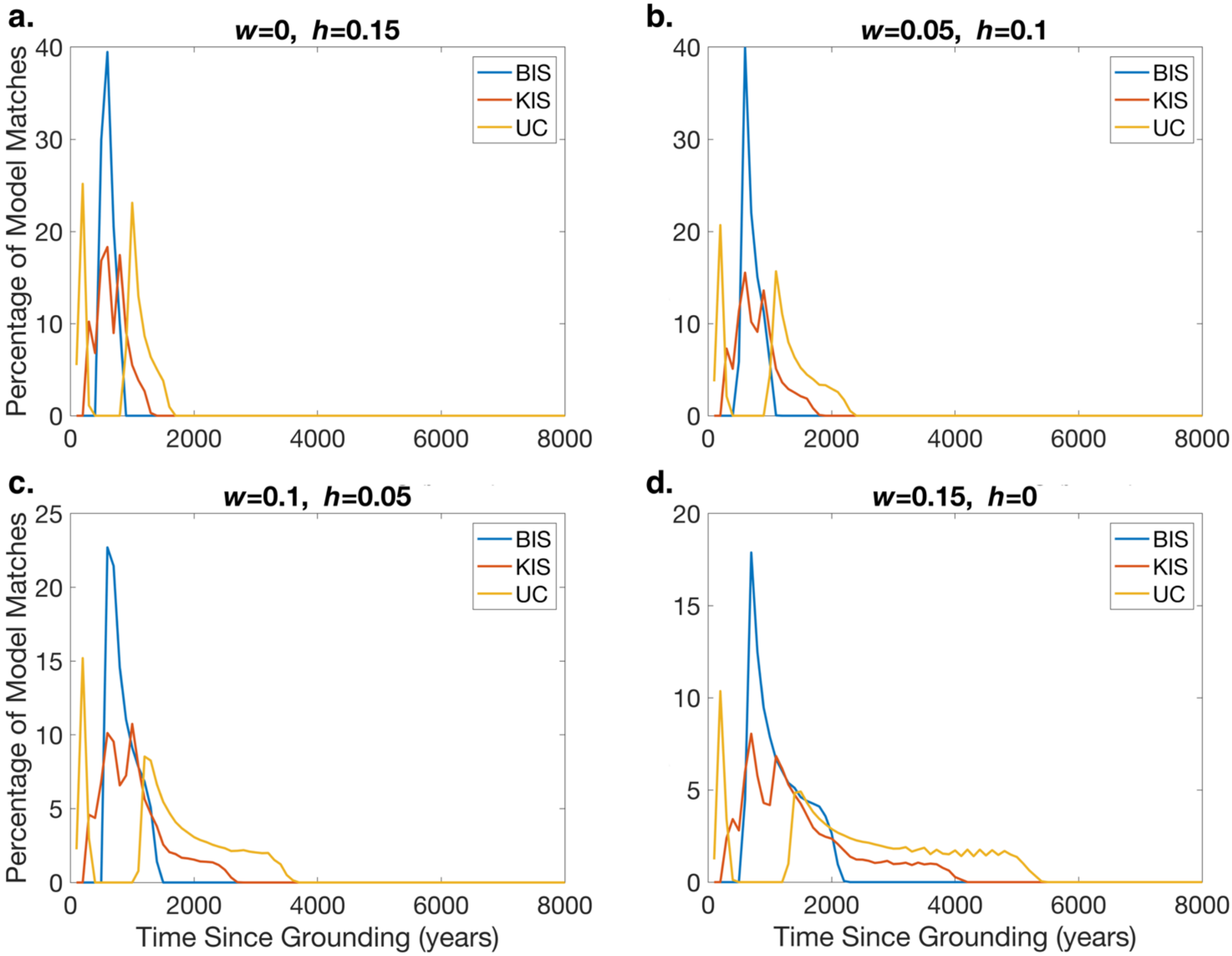

Figure S6: Sensitivity testing for phase 2 of the ice temperature model. Accumulation is kept constant at 0.15 m/yr. Accumulation is the sum of vertical velocity (*w*) and ice thickening (*h*).

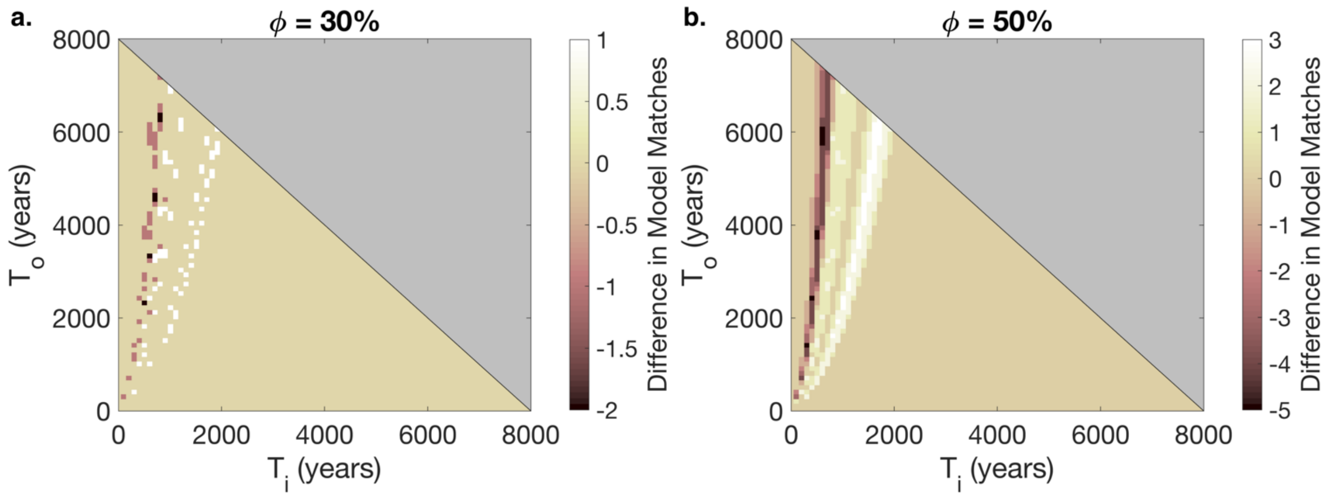

Figure S7: Sensitivity testing of ionic porewater diffusion model. In this scenario we varied sediment porosity (ϕ) to examine how much it would change the timing of grounding line readvance over SLW.

Table S1: Total Carbon (TC), Total Organic Carbon (TOC), Total Inorganic Carbon (TIC), Total Nitrogen (TN), C:N, and $\delta^{13}C$ measurements from sediments collected at our field sites. With the exception of the samples collected at UC (italicized), the samples were collected as sediment cores from below either grounded ice or ice shelf. The UC samples were sediments that were melted out of sediment-laden basal ice.

Core Name	Site	TC (w%)	TOC (w%)	TIC (w%)	TN (w%)	C_{org}:N (atom:atom)	$\delta^{13}C_{org}$ (‰)
RISP Core 7 4-6.6cm	RISP	0.5	0.2	0.3	0.07	3.8	-24.67
RISP Core 7 9.5-11cm	RISP	0.3	0.2	0.1	0.05	3.7	-25.60

RISP Core 7 20-21.5cm	RISP	0.5	0.4	0.1	0.07	6.0	-25.34
RISP Core 7 39-40.5cm	RISP	0.5	0.4	0.1	0.08	6.1	-25.00
RISP Core 7 64.5-66cm	RISP	0.6	0.4	0.2	0.08	6.6	-25.09
RISP Core 10 4-6cm	RISP	0.4	0.2	0.2	0.07	3.3	-25.48
RISP Core 10 13-14.5cm	RISP	0.4	0.2	0.2	0.07	3.8	-25.20
RISP Core 10 17.8-19.5cm	RISP	0.5	0.4	0.1	0.08	6.2	-25.38
RISP Core 10 39-41cm	RISP	0.6	0.4	0.2	0.07	6.6	-24.95
RISP Core 10 79.5-81cm	RISP	0.6	0.5	0.1	0.08	7.2	-25.26
SLW-PC1B	SLW	0.4	0.3	0.1	0.03	12.5	-25.39
SLW-PL0T	SLW	0.4	0.3	0.1	0.02	15.6	-24.90
SLW-PL1T	SLW	0.4	0.4	0.1	0.02	17.7	-24.84
89-4-0.3	WIS	0.4	0.3	0.0	0.02	16.6	-25.32
89-7-2T	WIS	0.3	0.3	0.1	0.02	14.3	-25.31
89-7-5T	WIS	0.4	0.3	0.0	0.02	17.6	-25.56
89-7-7T	WIS	0.4	0.3	0.1	0.03	15.3	-26.10
95-1-1-2	WIS	0.9	0.3	0.5	0.02	18.8	-25.56
95-5-1-3	WIS	0.4	0.4	0.0	0.02	19.3	-23.13
96-6-1-2C	KIS	0.5	0.5	0.0	0.02	25.2	-26.94
96-12-1-2-1-2	KIS	0.3	0.3	0.0	0.02	16.9	-25.19

93-14-1	*UC*	*0.2*	*0.2*	*0.0*	*0.02*	*9.7*	*-24.75*
96-9-1-1B	KIS	0.9	0.7	0.1	0.03	28.0	-25.78
95-1-1-2	WIS	0.4	0.3	0.1	0.03	13.9	-24.89
95-5-3-1	WIS	0.4	0.3	0.0	0.02	15.7	-25.27
96-6-1-21	KIS	0.6	0.5	0.1	0.03	19.5	-25.02
98-2-2-3C	BIS	0.9	0.7	0.3	0.03	23.8	-22.33
WGZ-GC1-08	WGZ	0.3	0.3	0.0	0.03	13.5	-24.39
WGZ-GC1-18	WGZ	0.2	0.2	0.1	0.02	8.9	-24.33
WGZ-GC1-28	WGZ	0.3	0.3	0.0	0.02	14.6	-24.63
WGZ-GC1-38	WGZ	0.3	0.2	0.1	0.02	10.7	-25.58
WGZ-GC1-48	WGZ	0.2	0.2	0.1	0.02	9.7	-22.44
WGZ-GC1-58	WGZ	0.3	0.2	0.1	0.03	10.1	-25.86
WGZ-GC1-63	WGZ	0.3	0.2	0.1	0.02	9.3	-25.44
93-10-1	*UC*	*0.2*	*0.1*	*0.0*	*0.02*	*7.4*	*-20.98*
95-3-2-4-1	WIS	3.2	0.4	2.8	0.02	20.3	-25.29